DOCUMENT CONTROL SHEET

	ORIGINATOR'S REF.		SECURITY CLASS.
	NLR-TP-2000-429		Unclassified

ORGINATOR
National Aerospace Laboratory NLR, Amsterdam, The Netherlands

TITLE
Short turn-around, parallel CFD to predict three-dimensional high-lift flows around a transport aircraft powered by ultra-high by-pass ratio turbofan engines

PRESENTED AT:
22nd ICAS Congress, Harrogate, United Kingdom, 27 August - 1 September 2000

AUTHOR	DATE	pp	ref
J.E.J. Maseland	September 2000	22	11

ABSTRACT
The use of new highly efficient engines with very- or ultra-high by-pass ratios will be of major importance for the development of new modified transport aircraft since they offer drastic reductions in fuel consumption, noise and emissions. The larger diameter of these engines in combination with requirements concerning ground clearance, landing gear height and weight leads to the necissity of a very close coupling with the wing. This is especially true for twin power-plant configurations. The resulting engine-airframe interference can lead to large maximum lift penalties for configurations with high-lift devices deployed and engines running at maximum take-off power.
The investigation of integrated high-lift capabilities is still based on wind tunnel testing and full scale flight testing since the corresponding flow problems are prime examples of complexity both in terms of geometry and flow physics. The demand for support from accurate flow simulations by short-turn-around computer codes is self evident since CFD methods offer the promise of providing comprehensive analysis of maximum lift phenomena witin the constraints of short time scales and reduced costs. Unstructured grid methods in combination with parallel computers are ideally suited to model highly complex geometries, have the potential to model detailed flow characteristics when adaptive grid strategies are incorporated and allow for sufficiently short computing times.
The present work demonstrates the feasibility of short-turn-around CFD to analyse the complex flow field around a complete twin-engine transport aircraft configured for take-off.

Nationaal Lucht- en Ruimtevaartlaboratorium
National Aerospace Laboratory NLR

NLR-TP-2000-429

Short turn-around, parallel CFD to predict three-dimensional high-lift flows around a transport aircraft powered by ultra-high by-pass ratio turbofan engines

J.E.J. Maseland

This report is based on a presentation held at the 22nd ICAS Congress, Harrogate, United Kingdom, 27 August - 1 September 2000.

Division:	Fluid Dynamics
Issued:	September 2000
Classification of title:	Unclassified

Summary

The use of new highly efficient engines with very- or ultra-high by-pass ratios will be of major importance for the development of new or modified transport aircraft since they offer drastic reductions in fuel consumption, noise and emissions. The large diameter of these engines in combination with requirements concerning ground clearance, landing gear height and weight leads to the necessity of a very close coupling with the wing. This is especially true for twin power-plant configurations. The resulting engine-airframe interference can lead to large maximum lift penalties for configurations with high-lift devices deployed and engines running at maximum take-off power.

The investigation of integrated high-lift capabilities is still based on wind tunnel testing and full scale flight testing since the corresponding flow problems are prime examples of complexity both in terms of geometry and flow physics [1].
The demand for support from accurate flow simulations by short-turn-around computer codes is self evident since CFD methods offer the promise of providing comprehensive analysis of maximum lift phenomena within the constraints of short time scales and reduced costs [9]. Unstructured grid methods in combination with parallel computers are ideally suited to model highly complex geometries, have the potential to model detailed flow characteristics when adaptive grid strategies are incorporated and allow for sufficiently short computing times [7].

The present work demonstrates the feasibility of short-turn-around CFD to analyse the complex flow field around a complete twin-engine transport aircraft configured for take-off.

Contents

(22 pages in total)

1 Introduction

The highly competitive global market drives the aerospace industry for increased economy and safety of their aircraft. Direct operating cost reductions are pursued through economies of scale, enhanced airframe aerodynamics, and advances in propulsion technology.

A significant part of the operating cost cut is achieved by the use of new low-operating-cost, high-reliability turbofan engines. The engines are characterised by very-high by-pass ratios with reduced fuel consumption, noise and emissions levels. They represent corner-stones in development programmes of new ultra-high capacity aircraft as well as in derivative programmes of existing aircraft in order to comply with more stringent environmental and ecological regulations.

The large fan diameter of these engines in context with requirements concerning ground clearance, landing gear height and weight leads to a very close coupling of the engine nacelle with the wing. (This is especially true for twin powerplant configurations.) The associated aerodynamic interference effects can result in a maximum lift penalty. An even closer coupling is required for a novel engine concept like the envisioned ducted propfan engine featuring an ultra-high bypass ratio and promising a further reduction of 10 - 15 % in fuel consumption. The design challenge for the cruise configuration is to maximise the performance increase potential through minimising the additional engine installation penalties [3].

Exploration of installation and jet interference effects of advanced engine concepts featuring extremely large fan-diameters has been carried out in the DUPRIN-2 project [3]. Understanding of the underlying flow phenomena has been obtained from wind tunnel tests complemented by numerical investigations based on structured grids. The main effort was focussed on installation effects at transonic conditions [2].

The next step in the systematic study comprises engine integration aspects at low speed. The deflection of slats and flaps introduces additional integration constraints for very close coupled engines. Potential maximum lift interference penalties arise for fully deflected slats and flaps at large incidence angles.

The time frame needed for the identification or understanding of the maximum lift penalties is highly relevant for airframe designers. In the quest for integrated high-lift design, they need to be able to account for these effects early in the design process. Optimisation of the engine location underneath a wing and compatibility verification for the high-lift configuration involves a significant number of individual cases to be considered.

The objective of the present work is to demonstrate the feasibility of short turn-around CFD based on unstructured meshes to analyse the high-lift flow field around the twin-engine ALVAST wind tunnel model with high-lift devices at a setting for take-off. Flow modeling aspects for a short turn-around time are addressed in a short description of the algorithmic components incorporated in the

FASTFLO CFD system [11]. The FASTFLO CFD system is employed for a numerical investigation to explore installation and jet interference effects of UHBR engines.

2 FASTFLO CFD system

The accuracy and turn-around-time aspects of aerodynamic analysis are particular challenging for integrated high-lift design. The flow modeling components address geometry modeling, grid generation, flow simulation and post-processing. Each of these components is required to be accurate, efficient and robust. Moreover, the time frame aspect requires the integration of these elements into a streamlined solution process.

The preparatory step for CFD analysis concerns the extraction of the CFD geometry from the CAD/CAM geometry. The CAD/CAM geometry may incorporate overlapping surfaces or geometrical details (e.g. small holes) that may be non-relevant for the flow problem at hand. Furthermore, the CFD geometry has to satisfy the requirement of 'air-tightness' which implies that gaps have to be closed.

Data exchange between the CAD/CAM system and the CFD system is based on a standardised format (IGES 5.1). The interface to the CFD system adds automatically topological information to the CFD geometry [4] for grid generation.

The discretisation the CFD geometry by means of triangular elements is based on an advancing front algorithm whereas the volumetric discretisation by tetrahedral elements is based on Delaunay type algorithm [10].

Maximum benefit of state-of-the-art computer architectures, like the shared-memory multi-vector processor machine NEC SX5/8B at NLR, is provided by a pre-processing algorithm. The element-based data structure is transformed to an edge-based data structure and the flow domain can be partitioned which allows for optimal vector and parallel performance of the flow calculation algorithm. Intercommunication and load balancing considerations have motivated the incorporation of the METIS algorithm [5] for grid partitioning. The algorithm minimises the number of edges cut by the partitioning under the constraint that the number of nodes is equal for each partition.

The flow solver advances the flow solution towards steady state using an explicit multi-stage Runge-Kutta time stepping method. Convergence acceleration is achieved by local time stepping and by employing a multi-grid procedure based on a control volume agglomeration technique. Data communication between multiple processors is based on the MPI library.

Propulsion simulation based on velocity extrapolation for the exhaust flow [6] proved to be more robust than pressure extrapolation [8] for high incidence angles in combination with low Mach numbers.

The CFD system incorporates a grid adaptation algorithm for local grid refinements. Gradient based refinement indicators of density, velocity and total pressure and total enthalpy are available. Node insertion on the actual aerodynamic surface is achieved by local surface spline reconstructions of the surface triangulation.

Since the inviscid flow modeling capability is an intermediate development stage, extension of the current flow modeling capability towards a viscous flow modeling capability is currently under way. The Reynolds-Averaged Navier-Stokes equations are then solved on a hybrid grid consisting of prismatic and tetrahedral elements. The prismatic elements are generated in the viscous dominated flow regions close to the aerodynamic surface.

3 Geometrical model

The geometrical model used in the present investigation is a representation of the wind tunnel model of the ALVAST high-lift configuration (see figure 1). The geometry represents a twin-powered transport aircraft with deployed slats ($\delta_s = 20^o$) and flaps ($\delta_f = 19.5^o$) at settings for take-off and is equipped with Ultra-High Bypass Ratio (UHBR) turbofan engines. The jet flow field of the engines is simulated by using turbine powered simulators where the fan is driven by pressurised air. The geometrical simplification made with respect to the actual wind tunnel model consists of neglecting the flap/slat tracks rendering the configuration as a multi-body geometry. The wing elements feature realistic trailing-edges with a finite thickness.

4 Numerical study

4.1 Grid generation aspects

Starting point for grid generation is a definition of the aerodynamic surface in terms of trimmed surfaces and curves established either from structured surface patches or IGES CAD entities. The mathematical description is required to be C^o continuous across adjacent surfaces. The present geometrical set-up is established by using available multi-block surface representations of an ALVAST high-lift model and a UHBR engine model. Installation of the engine underneath the multi-element wing required some geometry modeling with an external CAD tool (ICEM-CFD) to provide the trimmed surface patches at the slat-pylon and pylon-main-wing intersections (see figure 2). Note that the slats are modeled to intersect with the pylon.

The actual generation of the unstructured mesh entails the generation of a surface mesh with triangular elements and a volume mesh with tetrahedral elements. The user intervention in the highly automated grid generation process consists of the user-defined node density distribution for the entire flow domain. A single input-entry defines a uniform node spacing for the entire flow domain. Local mesh density refinements as required to resolve all geometrical length scales and the physics of the particular problem are defined with the aid of a graphical tool. The specification of the local node density is direct; it consists of the desired spacing between nodes and the distance over which the desired spacing has doubled.

The employed strategy for grid generation consists of generating a smooth and relative fine grid point distribution in the proximity of the aerodynamic geometry and a rapid decrease of the point density away from the configuration. This approach is based on the consideration that the initial surface discretisation has to resolve the local curvature adequately to allow for accurate surface grid refinement based on local spline reconstructions. Furthermore, the initial grid should be able to represent relevant flow phenomena in order to be identified by appropriate indicators for adaptive grid refinements thereby achieving an efficient grid point distribution.

Views of the initial surface grid are presented in figures 3 and 4 showing details of the wing/pylon/nacelle and the flap high-lift elements featuring 'blunt' trailing edges. The initial surface discretisation of the geometry consists of 736.555 triangular elements. The initial 3D grid contains 2.232.405 nodes which constitute 13.209.978 tetrahedral elements.

4.2 Engine installation and propulsion effects in high-lift flows

The high-lift flow around the ALVAST configuration for the flow condition $M_\infty = 0.22$, $\alpha = 12.03$ (degrees) is calculated based on the Euler equations. A second-order accurate AUSM upwind scheme is utilised for the computation of the convective fluxes. Convergence acceleration is achieved by employing 5 multi-grid levels. The wall clock time for the initial flow computation on

4 processors of the NEC SX5 amounts to two hours. A speed-up factor of about 3.7 is achieved by using 4 processors.

The surface pressure distribution is presented in figure 5 indicating the high suction levels near the leading edges which is a characteristic distribution in the low speed flight regime. The footprint of the vortices originating from the side-edge of the wing is visible.

The propulsion simulation at the Euler level of the turbofan engine involves the specification of uniform total pressure and temperature ratio's for the individual exhausts. For the present maximum take-off setting, the fan exhaust stream and the core exhaust stream feature higher total pressures and different total temperatures than the free stream. The fan exhaust stream expands into a jet with an increased Mach number (M_{fan}= 0.55) in a low speed ambient flow (M_{∞}= 0.22). The fan and core jets mix with each other as well as with the free stream flow and develop in an exhaust plume. Figure 6 shows the Mach number distribution in the vicinity of the UHBR engine. The velocity shear layer between the fan exhaust jet and the surroundig flow is observed on the pylon. The geometrical location and resolution of the fan exhaust boundary and resulting jet is extremely important for maximum lift phenomena. Accurate prediction of these effects entails minimisation of the mixing layer spreading due to artificial viscosity. Advantage is taken from an adaptive procedure to achieve local grid refinements. The results presented here are obtained on an adapted computational grid containing 3.082.438 nodes which constitute 17.735.250 tetrahedral elements. The wall clock time for the flow simulation on the adapted grid amounts less than one hour since the initial flow solution is interpolated onto the adapted grid. Grid adaptation is partially based on total enthalpy gradients to refine the grid at the location of the jet mixing layers. The interference of the fan exhaust jet and the deflected slats is indicated in the total enthalpy distribution presented in figure 7. The high total enthalpy levels associated to the fan exhaust jet on the slat show that the deflected slat protrudes into the fan exhaust jet. The close coupling of the engine and the wing dihedral result in a partial wetting of the inner lower wing surface by the fan exhaust jet (see figure 8). Figure 9 depicts that the spanwise flow in the slat cove is blocked by the pylon and is convected downstream in the corner established by the pylon and the wing.

4.3 Accuracy assessment in comparison with experiments

In order to assess the accuracy of the inviscid flow solutions for complex powered high-lift configurations, the numerical results are compared with experimental data obtained during wind tunnel tests in the DNW LLF facility. Keeping in mind the Euler equation approximation in the flow model, we expect that the pressure distribution on lower surface of the wing elements is well predicted since the boundary layer thickness is known to be small. Furthermore, the upper surface distribution is expected to be overpredicted in the flow calculation because of the camber reducing effect of the boundary layer. This is particular true for the main-wing element where the close-

coupled slat wake confluences with the upper-surface boundary layer.

Figures 11 through 14 show the comparison of computed and measured sectional surface pressure distributions for the individual high-lift elements. The location of the pressure-tab span-stations referred to as wing sections D1 - D9 are depicted in figure 10.

The comparison shows that the lower surface pressure distribution on all elements is already in good agreement with the experimental data (not considering wing sections D3 - D4). The upper surface pressure distribution on the main wing element is in fair agreement with the experimental data. The pressure distribution of the outer flap element is already in good agreement with the experimental data.

Effects of jet interference are observed at sections D3 - D4 where the stagnation pressure has a value larger than free stream reference value. This is an indication that the slat surface is wetted by the fan exhaust flow with a corresponding larger total pressure level than the onset flow. This observation is also an indication that the fan exhaust flow continues to expand under-neath the wing in the computation. Characteristic details of high lift flows are noticed at the outboard wing station D6 where the gap flow is visible as spikes in the leading edge pressure distribution of the main-wing-element.

5 Conclusions

The present work demonstrates the feasibility to analyse complex high-lift flows around a complete aircraft configured for take-off with a turn-around-time in the order of weeks.

The considered configuration is geometrically complex and simplifications with respect to the actual wind tunnel geometry concern the absence of slat and flap track fairings, rendering the configuration as a multi-body geometry.

The enabling technology for flow modeling around complex configurations with a short turn-around time is highly automatic surface triangulation and grid generation in the flow domain. The inherent flexibility of the unstructured grid technique allows for discretisation of flow domains with large variations in geometrical length scales. Furthermore, the control-volume agglomeration based multigrid technique allows for highly efficient parallel implementations that reduce the wall clock time for the flow simulation by a factor almost equal to the number of processors.

The unstructured CFD method incorporated in the FASTFLO CFD system is applied in a numerical investigation of engine integration and jet-interference effects of a novel engine concept featuring large fan diameters. The present results indicate that the deflected inner slat protrudes into the fan exhaust jet for large incidence angles during take-off.

The flow solver has shown a scalability of 91 % per processor on the NEC SX-5 shared-memory supercomputer.

The flow calculations are performed on the Euler equation level, being an intermediate stage of development towards a viscous flow modeling capability based on the Reynolds-Averaged Navier-Stokes equations.

6 Acknowledgement

The present investigation is carried out in the framework of the bi-lateral NLR-DLR co-operation on 'CFD for complete aircraft'. The Euler version of the CFD system has been initiated in the FASTFLO-I project (with partners DLR, FFA, DASA, SAAB, IBK).
The author acknowledges the support of DLR Braunschweig for providing the geometrical description of the ALVAST high-lift geometry.
The DNW experiment was carried out in the framework of the DUPRIN-II project.

7 References

1. Arnold F. Numerical flow simulation on high-lift configurations at Daimler-Benz aerospace airbus. *Proc 'High Lift and Separation Control' Royal Aeronautical Society*, No 8, 1995.
2. Burgsmuller W., Hoheisel H. and Kooi J.W. Engine-airframe interference on transport aircraft with ducted propfans -the European research program DUPRIN-. *Proc ICAS 1994*, No 3.7.1, 1994.
3. Burgsmuller W. and Rossow C. Installation of high-bypass-ratio engines on future transport aircraft. *Proc 7th European Propulsion Forum*, No 3.1, 1999.
4. De Cock K.M.J. and Van der Burg J.W. Surface triangulation based on IGES version 5.1. Technical Report TR-97076, NLR, 1997.
5. Karipis G. and Kumar V. Parallel multilevel K-way partitioning for irregular graphs. Technical Report 96-036, University of Minisota, 1996.
6. Kassies A. Inlet and outlet boundary conditions for the simulation of engines in the ENSOLV flow solver. Technical Report CR-95088, NLR, 1995.
7. Mavriplis D.J. and Pirzadeh S. Large-scale parallel unstructured mesh computations for 3D high-lift analysis. *Proc AIAA*, No 99-0537, 1999.
8. Rudnik R. Erweiterung eines driedimensionalen Eulerverfahrens zur Berechnung des Stroemungsfeldes um nebenstom Triebwerke mit Fan und Kernstrahl. Technical Report FB-91-13, DLR, 1991.
9. Szmelter J. and Cross R. Applications of unstructured meshes techniques to high-lift configurations. *Proc 'High Lift and Separation Control' Royal Aeronautical Society*, No 9, 1995.
10. Van der Burg J.W. Tetrahedral grid generation. Technical Report TR-98523, NLR, 1998.
11. Van der Burg J.W. and Oskam B. FASTFLO - Automatic CFD system for three dimensional flow simulations. Technical Report TP 97556 U, NLR, 1997.

8 Figures

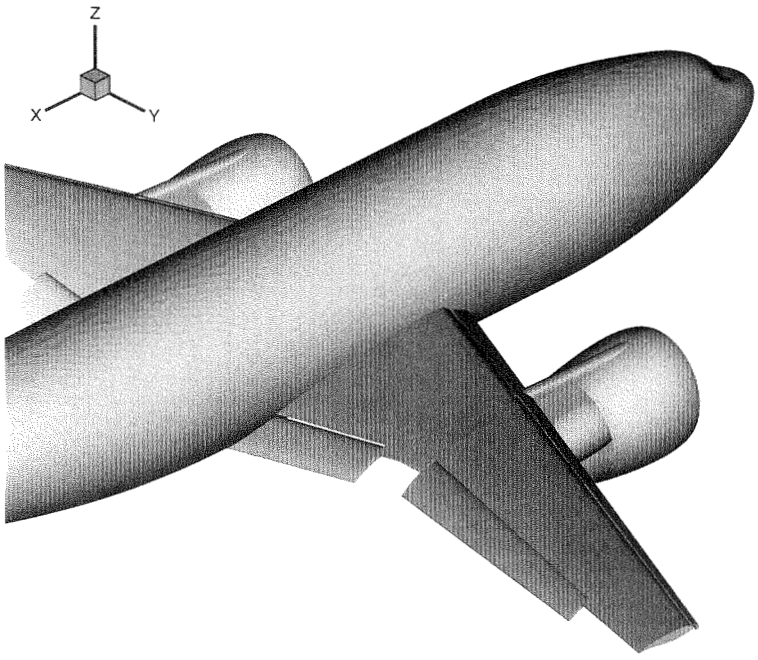

Fig. 1 ALVAST high-lift configuration equipped with UHBR engines (TPS)

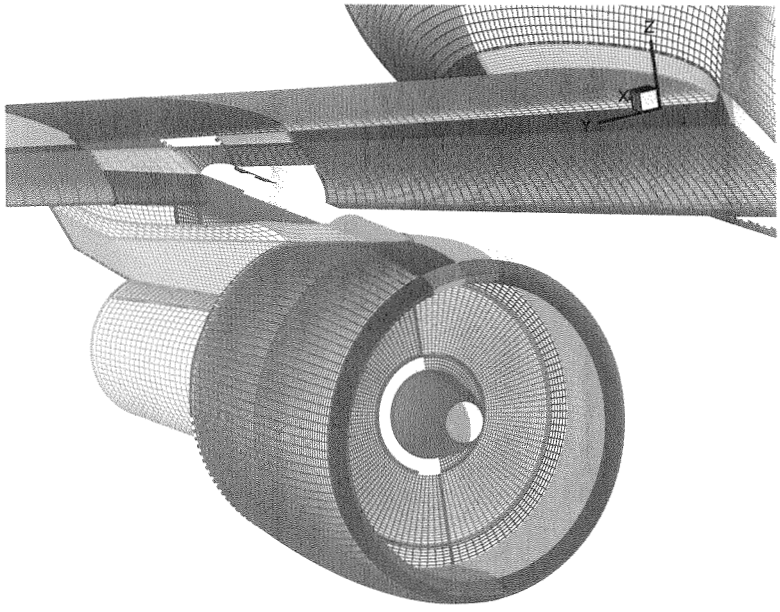

Fig. 2 Surface definition based on structured patches

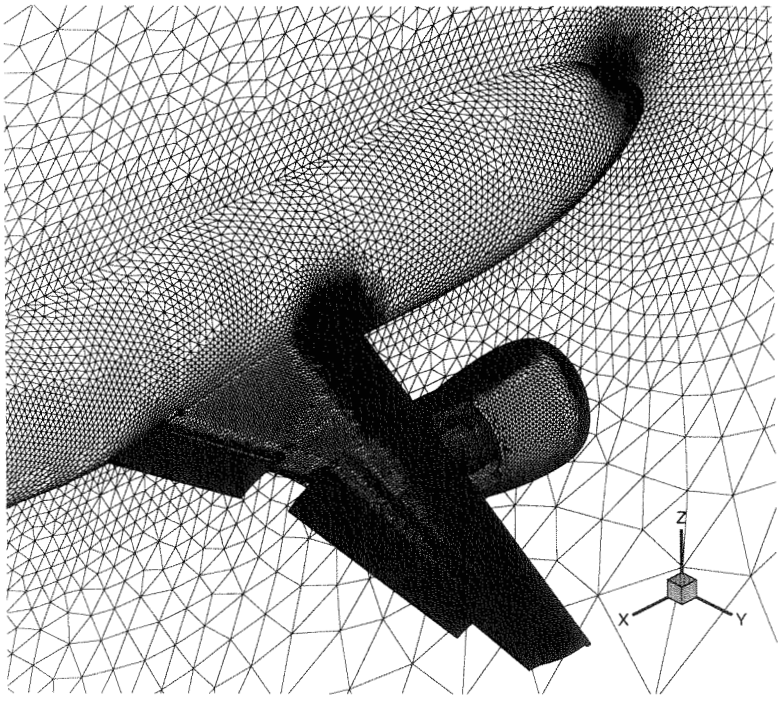

Fig. 3 Surface discretisation of the ALVAST high-lift configuration

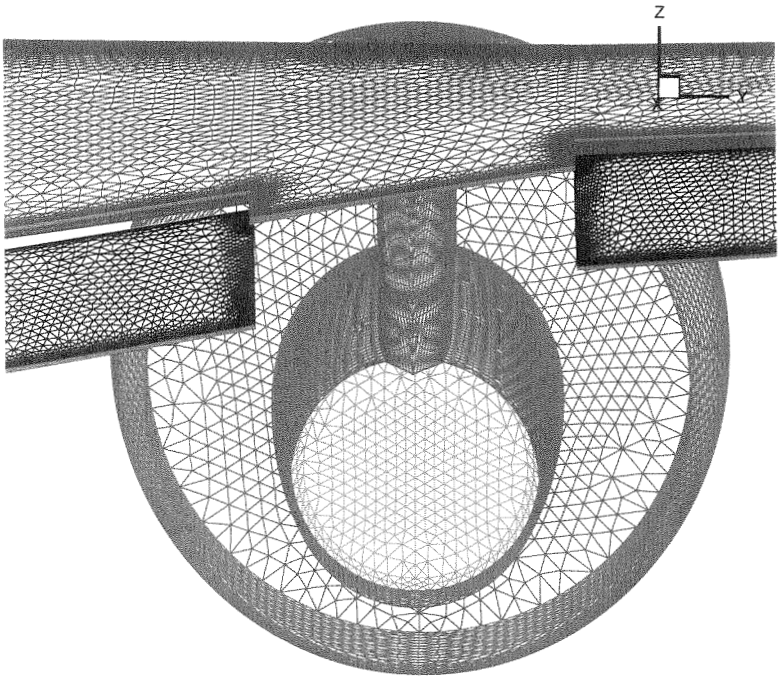

Fig. 4 Surface discretisation details for the deflected flaps, pylon and UHBR engine (rear-view)

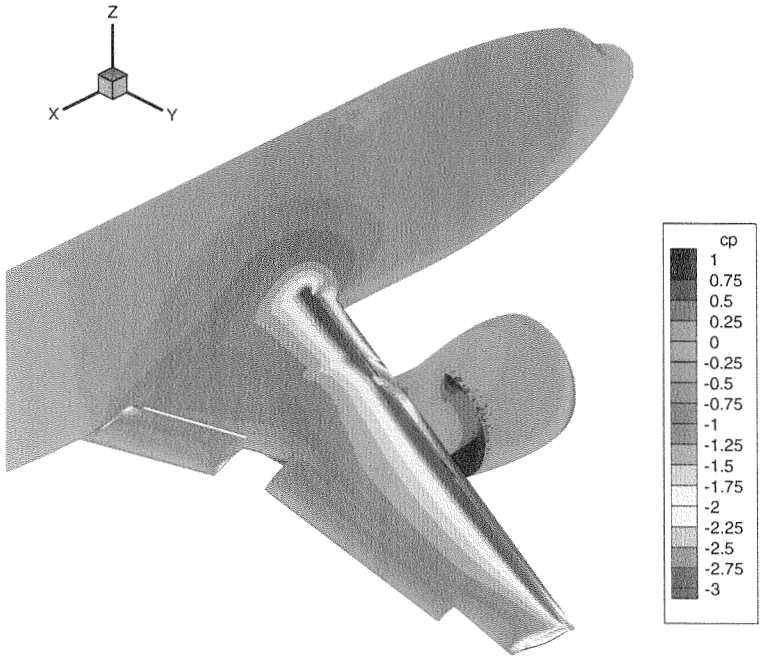

Fig. 5 Surface pressure distribution for the ALVAST configuration

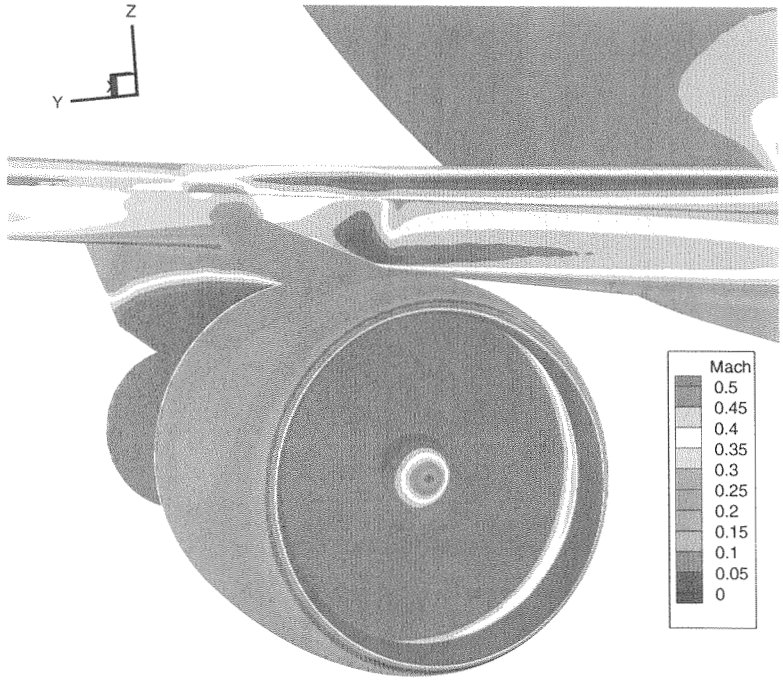

Fig. 6 Mach number distribution in vicinity of the UHBR engine

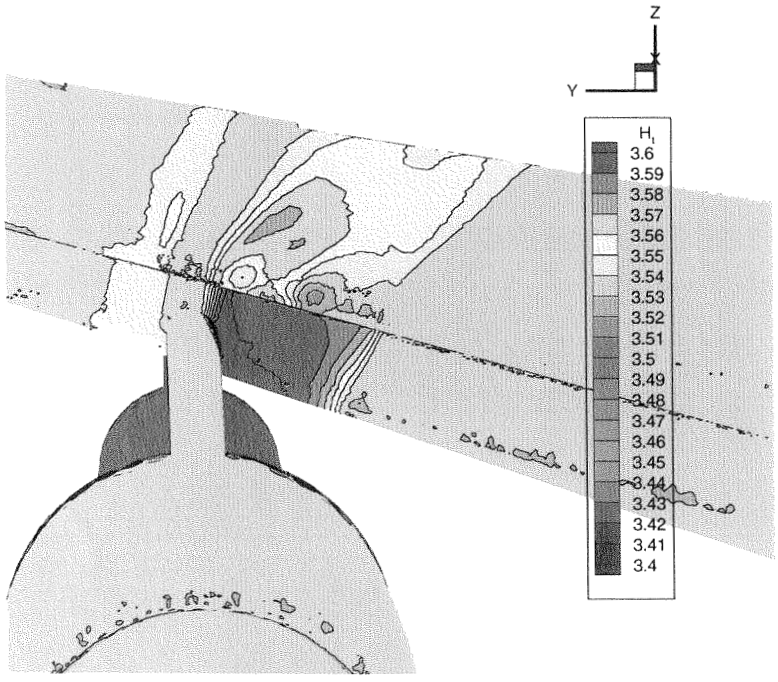

Fig. 7 Total enthalpy distribution indicating the jet interference of UHBR fan exhaust on the deflected slat

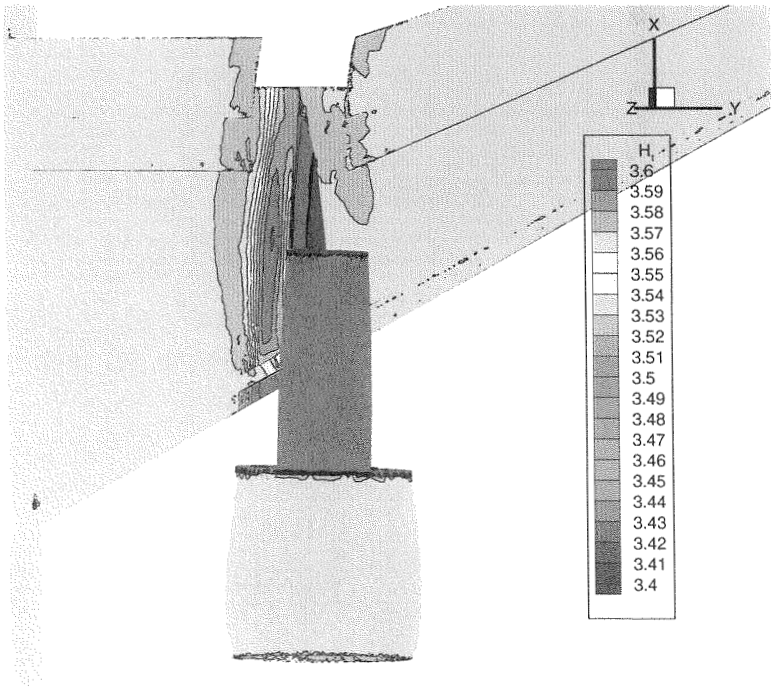

Fig. 8 Jet interference of UHBR fan exhaust on lower wing surface illustrated by total enthalpy distribution

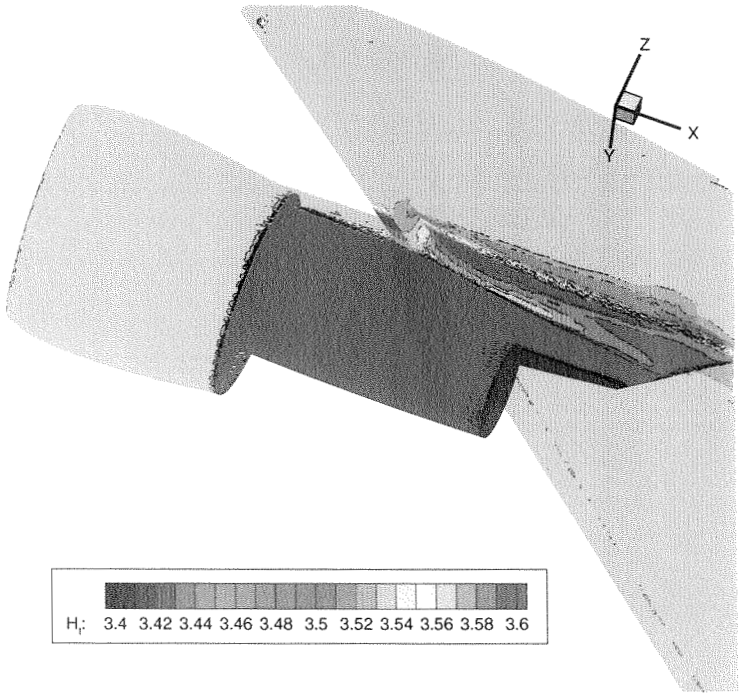

Fig. 9 Slat cove flow convection on lower wing surface depicted by total enthalpy distribution

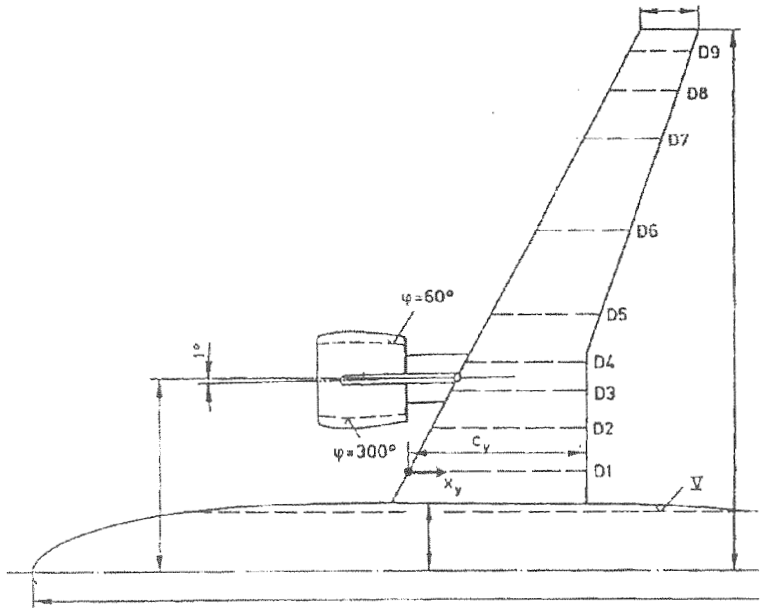

Fig. 10 Pressure tab locations on the ALVAST model in wing sections D1 through D9

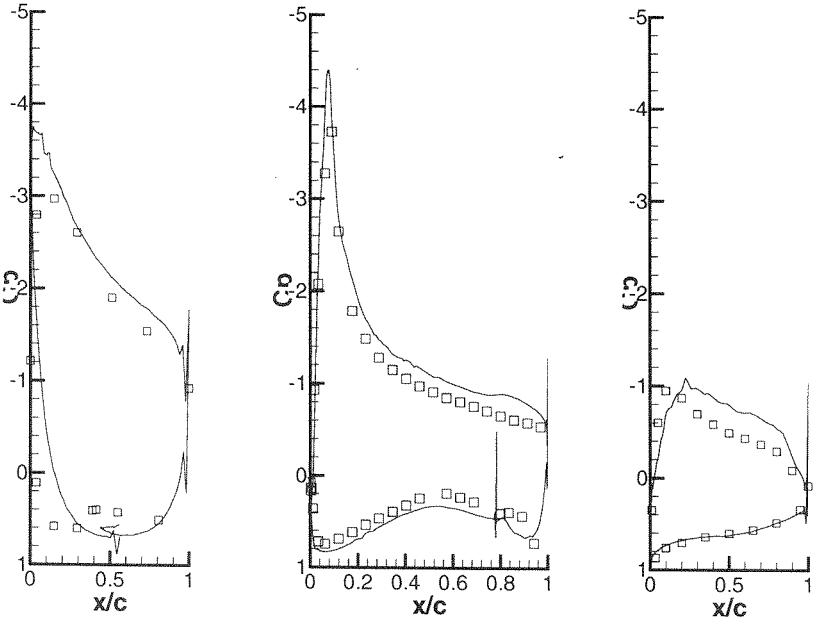

Fig. 11 Surface pressure distributions on the individual wing elements at section D2 (symbols represent DNW experiment)

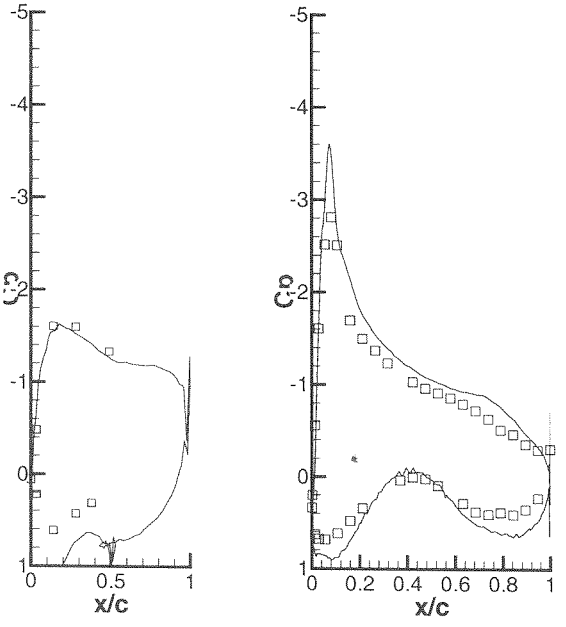

Fig. 12 Surface pressure distributions on the individual wing elements at section D3 (symbols represent DNW experiment)

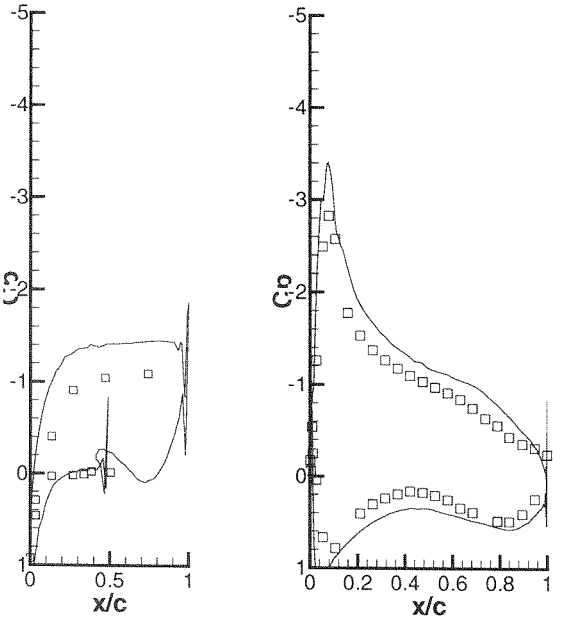

Fig. 13 Surface pressure distributions on the individual wing elements at section D4 (symbols represent DNW experiment)

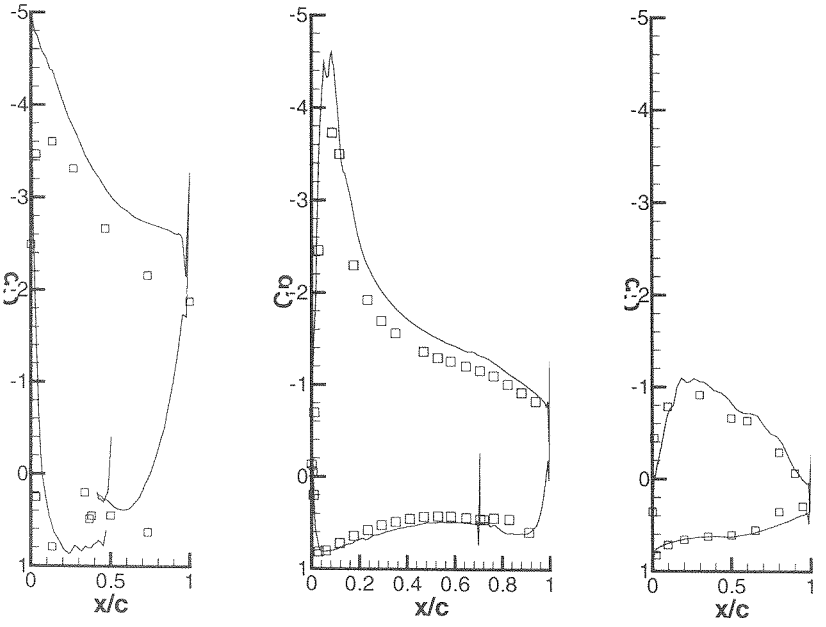

Fig. 14 Surface pressure distributions on the individual wing elements at section D6 (symbols represent DNW experiment)